Computational Materials Science 221 (2023) 112090

Contents lists available at ScienceDirect

Computational Materials Science

journal homepage: www.elsevier.com/locate/commatsci

Full length article

A computational method to estimate spin–orbital interaction strength in solid state systems

Qiangqiang Gu [a,b,*], Shishir Kumar Pandey [b,*], Rajarshi Tiwari [c]

[a] School of Mathematical Science, Peking University, Beijing, 100871, China
[b] AI for Science Institute, Beijing, 100871, China
[c] School of Physics, AMBER and CRANN Institute, Trinity College Dublin, Dublin, 2, Ireland

ARTICLE INFO

Keywords:
Spin–orbital interaction
Tight-binding model
Density-functional theory
Electronic structure

ABSTRACT

Spin–orbit coupling (SOC) drives interesting and non-trivial phenomena in solid-state physics, ranging from topological to magnetic to transport properties. A thorough study of such phenomena often requires effective models where the SOC term is explicitly included. However, the estimation of SOC strength for such models mostly depends on the spectroscopy experiments which can only provide a rough estimate. In this work, we provide a simple yet effective computational approach to estimate the onsite SOC strength using a combination of the *ab initio* and tight-binding calculations. We demonstrate the wider applicability and high sensitivity of our method by estimating SOC strength of materials with varying SOC strengths and the number of SOC active ions. As examples, we consider strongly correlated, topological, and semiconducting materials. We show that the estimated strengths agree well with the proposed values in the literature lending support to our methodology. This simplistic approach can readily be applied to a wide range of materials.

1. Introduction

The spin–orbit coupling (SOC), a relativistic interaction that couples electronic spin ($\boldsymbol{S}$) and its orbital momentum ($\boldsymbol{L}$) in an atom, causes the splitting of electronic terms into multiplets with total angular momentum $\boldsymbol{J} = \boldsymbol{L} + \boldsymbol{S}$. Dependence of SOC strength λ on the atomic number Z as $\sim Z^4$ make this interaction non-perturbative and crucial in heavier elements for accurate description of their electronic structure. When these elements are put in a crystal, the situation becomes complex as other splitting terms like crystal field (CF) take part in determining the electronic structure of a solid. Nevertheless, SOC still manifests its vital role in materials in the form of various interesting physical phenomena. Some of the examples are magnetic anisotropy [1–3], spin current [4], anomalous Hall effect [5–8] and the topological properties of materials originating from SOC effects [9–16]. Most recently, in strongly correlated materials, the interplay of SOC with other electronic interactions like Coulomb interaction and crystal fields have given rise to exotic phases like unconventional superconductivity [17–20] and Kitaev interactions for the realization of quantum spin liquid state [21,22]. Additionally, in 2D materials such as transition metal dichalcogenides (TMDCs), SOC effects can be crucial for possible valleytronic and spintronic applications [23]. Given that SOC can strongly modify the electronic structure near the Fermi level resulting in drastic changes in charge carrier mobility and transport properties, its implications in the context of device-based applications are also numerous. Thus, SOC effects are imperative for the electronic structure modeling of materials in condensed matter physics.

From the computation perspective of materials modeling, SOC effects can be self-consistently included in highly accurate Density Functional Theory (DFT) based *ab initio* methods. However, in many cases such as strongly-correlated materials or large-scale systems, the application of DFT becomes infeasible. A workaround in such cases is the construction of an effective model e.g. tight-binding (TB), multiband Hubbard–Kanamori [24] or Kane–Mele models [25], which can closely describe materials properties of interest. Such models have further advantages like their low computation cost, flexibility to explicitly include additional interactions, and varying their strengths to examine the corresponding effects on materials properties. As a specific example, one can consider the Hamiltonian $H = H_{\mathrm{TB}} + H_{\mathrm{CF}} + H_{\mathrm{soc}} + H_{\mathrm{int}}$, where first, second, third and fourth terms correspond to hoppings, CF, SOC, and Hubbard–Kanamori interaction terms. This model quite accurately describes the energy spectrum of spin–orbit coupling excitations observed in Resonant Inelastic X-ray scattering (RIXS) experiments, and also can be used to estimate the strength of Kitaev magnetic interactions (originating from SOC effects) in so-called spin–orbit coupling assisted Mott insulators [26,27]. One can also vary SOC strength λ ($H_{\mathrm{soc}} = \sum_i \lambda_i \boldsymbol{L}_i \cdot \boldsymbol{S}_i$, i is atomic index) within these models to see its effect on

* Corresponding authors
E-mail addresses: guqq@pku.edu.cn (Q. Gu), shishir.kr.pandey@gmail.com (S.K. Pandey).

https://doi.org/10.1016/j.commatsci.2023.112090
Received 1 December 2022; Received in revised form 15 February 2023; Accepted 17 February 2023
Available online 27 February 2023
0927-0256/© 2023 Elsevier B.V. All rights reserved.

the properties of interest in a material. [27]. Available techniques like constrained random-phase-approximation (cRPA) [28–30] and tight-binding can estimate the strength of Coulomb interaction U, Hund's coupling J_H, hopping amplitudes t and CF strength Δ^{CF} [26,27,31].

However, for the estimation of λ, one mostly relies on the experiments like low-temperature transport spectroscopy, absorption spectroscopy, electroreflectance measurements. Such an estimation of λ, in many cases, may be erroneous. It is because, firstly, spectral features of a solid used to estimate λ may not be solely emerging from SOC effects and more often than not influenced by other structural aspects. This can lead to an "effective" SOC in materials. This is consistent with the fact that in solids with moderate SOC interaction, the atomistic approach to determine the strength of SOC cannot be straightforwardly applied. For example, as shown by one of us [27] that experimental estimation from SOC-assisted excitations brings $\lambda = 15$ meV for Co^{+2} ions in cobaltates and yet our computationally estimated value $\lambda = 65$ meV reproduces experimental features quite well.

Secondly, these structural features (e.g. trigonal or tetragonal distortion of an octahedra) may have large variations in different materials implying that effective SOC may also significantly vary. However, in the absence of optical measurements for a particular material, one often has to choose the value of λ from a broad range available from experiments on other materials belonging to similar classes rather than the material of interest itself. Given that λ depends on the ionic and spin state of the corresponding atom in a solid as well as other structural aspects, such a choice of λ may be amiss or erroneous. Several attempts have been made in the past including some very recent ones to validate and estimate the onsite-SOC interaction in isolated atoms, monoatomic crystals, and binary compounds [32–35]. However, a general procedure for the estimation of λ which can readily be applied to any material of interest is still missing. Computationally, *ab initio* calculations with Wannierization procedure [31,34] can produce the models that contain the SOC effect. However, in this case, the obtained Wannier orbitals are not necessarily the eigenstates of $\hat{S}_z$ and so, it will be cumbersome to extract λ from such models making their analysis and transferability an issue.

In this paper, we present a simple yet effective method to obtain the strength of SOC for any number of atomic species present in a material. Our method is based on a combination of *ab initio* and Wannier function-based tight-binding models (dubbed TBSOC [36] hereafter). In this method, we construct a full SOC Hamiltonian defined in the $|\ell, s_z\rangle$ basis, which is then used to fit the *ab initio* band structure where the SOC effect is self-consistently introduced. SOC strength is then estimated by fitting the *ab initio* eigenvalues within our model. After introducing the methodology, TBSOC is then tested considering various materials ranging from having weak ($3d$) to strong ($5d$) single SOC active ions. We also consider examples of, a topological material with two SOC active ions and two semiconductors, Si and GaAs, in which the strength of SOC significantly differs. The estimated SOC strength for this broad variety of materials is in close agreement with the values found in the literature which demonstrate the capability and the wide applicability of our method. We also show that the choice of the local coordinate system does not affect the results, and the model obtained in this form can further be utilized for additional analysis. These results demonstrate that our TBSOC method offers a direct and convenient way to estimate the strength of SOC in materials.

2. Methodology

In this section, we first discuss the theoretical background required for the implementation of TBSOC followed by the methodological procedure next.

Table 1
The cubic harmonics basis functions $X_{\ell m}$.

ℓ	$X_{\ell m}$	
$\ell = 0$	$X_{0,0} = \|s\rangle$	$= \sqrt{1/4\pi}$
$\ell = 1$	$X_{1,-1} = \|p_y\rangle$	$= \sqrt{3/4\pi} \cdot y/r$
	$X_{1,0} = \|p_z\rangle$	$= \sqrt{3/4\pi} \cdot z/r$
	$X_{1,1} = \|p_x\rangle$	$= \sqrt{3/4\pi} \cdot x/r$
$\ell = 2$	$X_{2,-2} = \|d_{xy}\rangle$	$= \sqrt{15/4\pi} \cdot xy/r^2$
	$X_{2,-1} = \|d_{yz}\rangle$	$= \sqrt{15/4\pi} \cdot yz/r^2$
	$X_{2,0} = \|d_{z^2}\rangle$	$= \sqrt{5/16\pi} \cdot (3z^2 - r^2)/r^2$
	$X_{2,1} = \|d_{xz}\rangle$	$= \sqrt{15/4\pi} \cdot xz/r^2$
	$X_{2,2} = \|d_{x^2-y^2}\rangle$	$= \sqrt{15/16\pi} \cdot (x^2 - y^2)/r^2$

2.1. Theoretical background

The TB Hamiltonian for materials can be described in the form as,

$$H_{TB} = \sum_{i\alpha,j\beta} T_{i\alpha,j\beta} c^{\dagger}_{i\alpha} c_{j\beta} + c.c. \tag{1}$$

where the $T_{i\alpha,j\beta}$ are the hopping elements (when $i \neq j$) or onsite element (when $i = j$) between the basis orbitals $|i\alpha\rangle$ and $|j\beta\rangle$. Here i, j are the atomic indices and α, β label the orbital basis functions. These basis functions can be described in terms of either spherical harmonics (Y^m_ℓ) or cubic harmonics ($X_{\ell m}$) and the two bases are interchangeable using the following unitary transformations.

$$X_{\ell m} = \begin{cases} \frac{i}{\sqrt{2}} \left(Y^{-|m|}_\ell - (-1)^m Y^{|m|}_\ell \right) & m < 0 \\ Y^0_\ell & m = 0 \\ \frac{1}{\sqrt{2}} \left(Y^{-|m|}_\ell + (-1)^m Y^{|m|}_\ell \right) & m > 0 \end{cases} \tag{2}$$

Above, ℓ and m are the angular and magnetic quantum number respectively. However, for efficient computational implementation, the cubic harmonic form of orbital basis functions are often considered, functional forms of which are listed in Table 1.

The SOC interaction that couples orbital momentum with that of spin can be accurately approximated by a local "atomic" contribution of form,

$$H_{soc} = \sum_i \lambda_i \boldsymbol{L}_i \cdot \boldsymbol{S}_i = \sum \lambda \left[\hat{L}_z \hat{S}_z + \frac{1}{2} \left(\hat{L}_+ \hat{S}_- + \hat{L}_- \hat{S}_+ \right) \right] \tag{3}$$

$\boldsymbol{L}_i$ and $\boldsymbol{S}_i$ are the angular and spin momentum operator, and $\hat{L}_\pm$, $\hat{S}_\pm$ are the corresponding raising and lowering operators. Since we are discussing the onsite operators for each site in the crystal, index i is drooped in the right hand side of Eq. (3). The operation of orbital angular momentum operators on the spherical harmonics Y^m_ℓ yields,

$$\begin{aligned} L_\pm Y^m_\ell &= \hbar \sqrt{\ell(\ell+1) - m(m \pm 1)} Y^{m\pm1}_\ell \\ L_z Y^m_\ell &= \hbar m Y^m_\ell . \end{aligned} \tag{4}$$

The same is also applicable to spin operators. From Eqs. (2)–(4), one can obtain the SOC Hamiltonian matrix in the Hilbert subspaces for p and d orbitals considering the basis functions $\alpha/\beta = [p_z, p_x, p_y]$ and $[d_{z^2}, d_{xz}, d_{yz}, d_{x^2-y^2}, d_{xy}]$ respectively. One should note that we have not considered spin index in the TB Hamiltonian given in Eq. (1) and a full Hamiltonian $\mathcal{H} = H_{TB} + H_{soc}$ can be constructed as $\mathcal{H} = \mathcal{I}_2 \otimes H_{TB} + H_{soc}$, where $\mathcal{I}_2$ is the two-dimensional identity matrix and $\otimes$ is the Kronecker product. The complete basis then becomes, $[p_{z\uparrow}, p_{x\uparrow}, p_{y\uparrow}, p_{z\downarrow}, p_{x\downarrow}, p_{y\downarrow}]$ and $[d_{z^2\uparrow}, d_{xz\uparrow}, d_{yz\uparrow}, d_{x^2-y^2\uparrow}, d_{xy\uparrow}, d_{z^2\downarrow}, d_{xz\downarrow}, d_{yz\downarrow}, d_{x^2-y^2\downarrow}, d_{xy\downarrow}]$. Thusly constructed H_{soc} for p and d orbitals are given in Eqs. (5) and (6) in Box I. Here, λ_p and λ_d are the SOC strength of atomic p and d orbitals.

$$H^{p}_{\mathrm{soc}} = \frac{\lambda_p}{2}\begin{pmatrix} 0 & 0 & 0 & 0 & -1 & i \\ 0 & 0 & -i & 1 & 0 & 0 \\ 0 & i & 0 & -i & 0 & 0 \\ 0 & 1 & i & 0 & 0 & 0 \\ -1 & 0 & 0 & 0 & 0 & i \\ -i & 0 & 0 & 0 & -i & 0 \end{pmatrix} \tag{5}$$

$$H^{d}_{\mathrm{soc}} = \frac{\lambda_d}{2}\begin{pmatrix} 0 & 0 & 0 & 0 & 0 & 0 & -\sqrt{3} & i\sqrt{3} & 0 & 0 \\ 0 & 0 & -i & 0 & 0 & \sqrt{3} & 0 & 0 & -1 & i \\ 0 & i & 0 & 0 & 0 & -i\sqrt{3} & 0 & 0 & -i & -1 \\ 0 & 0 & 0 & 0 & -2i & 0 & 1 & i & 0 & 0 \\ 0 & 0 & 0 & 2i & 0 & 0 & -i & 1 & 0 & 0 \\ 0 & \sqrt{3} & i\sqrt{3} & 0 & 0 & 0 & 0 & 0 & 0 & 0 \\ -\sqrt{3} & 0 & 0 & 1 & i & 0 & 0 & i & 0 & 0 \\ -i\sqrt{3} & 0 & 0 & -i & 1 & 0 & -i & 0 & 0 & 0 \\ 0 & -1 & i & 0 & 0 & 0 & 0 & 0 & 0 & 2i \\ 0 & -i & -1 & 0 & 0 & 0 & 0 & 0 & -2i & 0 \end{pmatrix} \tag{6}$$

Box I.

2.2. Implementation

Having obtained the H_{SOC} in previous section, as the next step, we now describe the complete process for the extraction of SOC strength in solid state materials. The procedure can be divided into mainly three sequential *steps* given below.

1. Non-spin polarized *ab initio* band structure calculation and its Wannier based TB Hamiltonian (H_{TB}).
2. Self-consistently SOC included *ab initio* band structure calculation.
3. Obtain the optimized SOC strength λ by fitting the band structure of *step* 2 with Hamiltonian $H_{\mathrm{TB}} + H_{\mathrm{SOC}}$ (of Section 2.1).

In *step* 3, the derivatives free Nelder–Mead optimization algorithm [37, 38] is used for error minimization when fitting the *ab initio* eigenvalues to obtain the SOC strength λ.

2.3. Ab initio calculations

In *steps* 1 and 2 of section Section 2.2, the *ab initio* band structure calculations can be performed with any of the available DFT packages with an interface to Wannier90 [39]. In this paper, we choose Vienna *ab initio* simulation package [40] for the calculations. Projector-augmented wave method [41,42] implemented within VASP (version-5.4.4) with the generalized-gradient approximation (GGA) within Perdew–Burke–Ernzerhof framework [43] is used and the energy convergence criteria in our self-consistent calculations are when the energy difference between successive steps was better than 10^{-5}/unit cell. Details of the plane wave energy cutoff and k-grid used for specific materials is provided in their respective sections.

To summarize our proposed methodology, our TBSOC program takes in a Wannier function based TB model (H_{TB}) and constructs the full Hamiltonian $\mathcal{H} = H_{\mathrm{TB}} + H_{\mathrm{soc}}$ by adding the onsite H_{soc} term. Starting with a random guess initial value of SOC strength λ, we fit the eigenvalues of SOC included *ab initio* band structure with $\mathcal{H}$. Error minimization of the fit then leads to corresponding λ for the atomic species of interest in a material.

3. Applications

Having described the methodology in detail, in this section we show the application of TBSOC on some transition metal compounds as well as on a topological and two semiconducting material. The transition metal compounds considered here are typical examples of magnetic materials belonging to $3d$, $4d$ and $5d$ classes, whose SOC strength ranges from weak to strong. The topological material (TaAs) we consider here is a typical example of non-magnetic and inversion symmetry broken Weyl semi-metal. The interesting magnetic or topological properties originating from SOC in these materials make them suitable candidates to test our method.

3.1. The case of transition metal compounds

In this section, as case studies, we demonstrate the estimation of λ in the various transition metal compounds. The choice of materials here is based on three points. First, keeping in mind that SOC strength λ depends on the number of valence electrons (the ionic state of the atom species of interest in a compound). Hence, we choose $Na_2TeCo_2O_6$ (Co^{+2}-$3d^7$) and α-$RuCl_3$ (Ru^{+3}-$4d^5$) as our example systems. Second, given a fixed number of valence electrons, λ changes with atomic number of species of interest. Hence, we show a comparison between iso-electronic α-$RuCl_3$ (Ru^{+3}-$4d^5$) and Na_2IrO_3 (Ir^{+4}-$5d^5$). Third, our choice is also based on the drastic variation of the SOC strength in these materials, which in different cases compete with other interactions likes the trigonal/tetragonal crystal field splitting. The magnitude of such splitting in these materials is believed to be in the range 10 meV–40 meV [44] and the SOC strength λ is either comparable or larger than the range of these splitting in the aforementioned compounds. This shows the effectiveness of our methodology apart from its diverse applicability.

As the first example, we showcase the results for α-$RuCl_3$. For the *ab initio* calculations, we have considered the experimentally observed crystal structure with monoclinic space group $C/2m$ [45–47], the crystal structure of which is shown in Fig. 1(a). We used plane wave

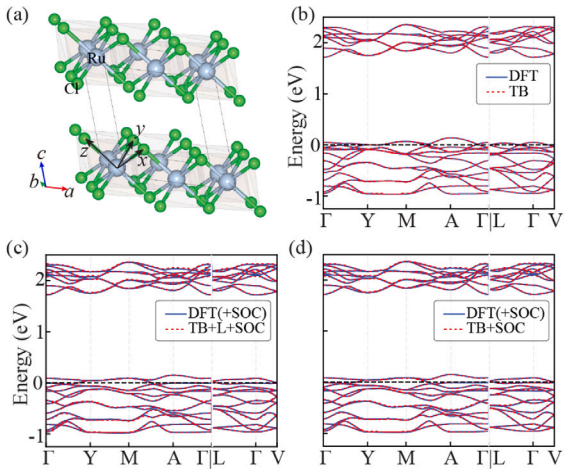


Fig. 1. (a) Crystal structure of α-$RuCl_3$. Light blue and green balls represent Ru and Cl atoms respectively. *a*, *b* and *c* are the crystallographic axes while *x*, *y* and *z* are the local octahedral coordinate axes. Edge-shared Ru-Cl_6 octahedrons are evident. (b) Wannier interpolation of the non-spin polarized *ab initio* band structure of α-$RuCl_3$ to obtain H_{TB}. All the five *d* orbitals of Ru are considered in the basis. (c) and (d) show the fitting of SOC included *ab initio* band structure with $H_{TB} + H_{SOC}$ in two cases, with (TB+L+SOC) and without (TB+SOC) local octahedral coordinate system respectively. Fermi energy is set to zero.

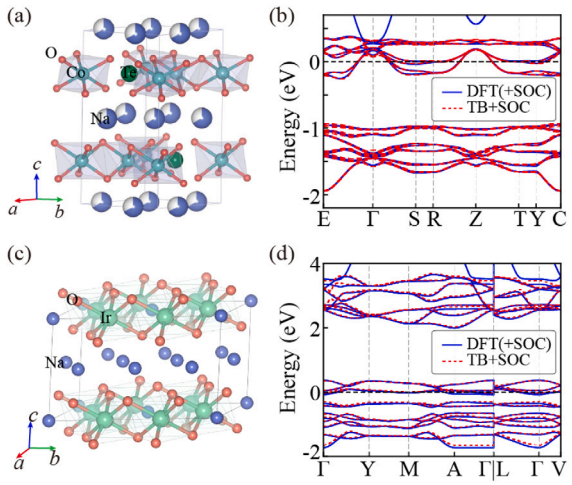


Fig. 2. (a) and (c) Crystal structure of $Na_2TeCo_2O_6$ and Na_2IrO_3. The white-blue ball in (a) represents partial occupancy of the Na sites. *a*, *b* and *c* are the crystallographic axes. Cyan/green and red balls represent Co/Ir and oxygen atoms respectively. Edge-shared Co/Ir-O_6 octahedrons are evident in (a) and (c). (b) and (d) show the fitting of SOC included *ab initio* band structure with a tight binding model after including onsite spin–orbit coupling term for $Na_2TeCo_2O_6$ and Na_2IrO_3 respectively. All the five *d* orbitals are considered in a tight binding basis in both these cases. Fermi energy is set to zero.

energy cutoff 500 eV and Γ-center *k*-grid of 6 × 3 × 6 in our DFT self-consistent calculations. The rest of the calculation details are the same as described earlier in Section 2.3. The layered structure with edge-shared Ru-Cl_6 octahedron is evident from this figure. As described in Section 2, in the first step, we construct a TB Hamiltonian (H_{TB}) using Wannier interpolation of the non-spin polarized *ab initio* band structure, and the plot is shown in Fig. 1(b). One can see a very good agreement between the two band structures from this figure. This gives us the confidence to proceed to the second step in which we calculate the *ab initio* band structure with SOC included at the self-consistent level. We then fit this relativistic band structure with H_{TB} after adding the onsite SOC H_{soc} term. A plot of this fitting procedure is shown in Fig. 1(c). We have emphasize here that in both the cases in Fig. 1(b) and (c) we use the local octahedral coordinate system shown in Fig. 1(a) to obtain H_{TB}. It is also possible to obtain the estimate of λ is the global crystallographic coordinate axes and the fitting procedure is not affected by the choice of coordinate settings. This is evident from Fig. 1(d) where the H_{TB} obtained in global coordinates is used for the fitting. The estimated value of λ in both cases is ∼ 0.120 eV. This value of λ, though in close agreement, is slightly larger by 20 meV from previously experimentally estimated value [48,49]. As explained in the introduction, underestimation of λ from experiments may come from other structural distortions at play. We emphasize here that further analysis of the tight-binding model, often required to understand the electronic properties of the material, is not straightforward when the global coordinate is used in the honeycomb lattice systems. Hence, we recommend the use of a local coordinate system in such cases.

In order to demonstrate the sensitivity of our method, following the same the procedure, we estimate λ for two more cases, namely for $Na_2TeCo_2O_6$ and Na_2IrO_3. For these two cases, the strength of SOC varies drastically for Co^{+2} and Ir^{+4} ions. We consider the crystal structure of $Na_2TeCo_2O_6$ with space group $P6_322$ [50–55] and Na_2IrO_3 with $C2/m$ [56–58] which are shown in Fig. 2(a) and (c) respectively. We used plane wave energy cutoff 550 eV and Γ-center *k*-grid of 8 × 8 × 4 for $Na_2TeCo_2O_6$ and 8 × 6 × 8 for Na_2IrO_3 in our DFT self-consistent calculations. The rest of the calculation details are the same as described earlier in Section 2.3. The fitting of the SOC included *ab initio* band structure in these two materials is shown in Fig. 2(b) and (d). One can see a very good fitting is obtained in both cases. Estimated values of λ are 0.065 eV for $Na_2TeCo_2O_6$ and 0.380 eV for Na_2IrO_3 which matches well with the previous experimental estimation [59].

In this section, we have considered examples in which there was only one spin–orbit coupling-activated transition metal ion present. However, there can be more than one atomic species in a material with active spin–orbit coupling interaction. To demonstrate the applicability of our method in such cases as well, we consider an example of a topological material, namely TaAs in the next section.

3.2. The case of topological material

TaAs have been theoretically predicted [15] and experimentally proven to be a topological Weyl semi-metal [60]. Its thoroughly studied topological properties such as the surface Fermi arcs [15], edge states [61], surface-bulk connectivity [62], chiral anomaly [63] and non-linear optical responses [64] are driven by the SOC effects. In TaAs, which crystallizes in a body-centered-tetragonal structure as shown in Fig. 3(a) with the non-centrosymmetric space group $I4_1md$, both, the Ta (*d*) and As (*p*) are considered to be SOC-active atoms. Hence, to describe this system, one needs to construct the full Hamiltonian $\mathcal{H}$ as explained earlier containing both the atoms and their corresponding SOC active orbitals. The H_{TB} model in $\mathcal{H}$ is again obtained from non-spin polarized DFT calculation with the Wannier interpolation procedure considering As-*p* and Ta-*d* orbitals in the basis. Plane wave energy cutoff is set to be 500 eV and Γ-center *k*-grid of 10 × 10 × 4 are used in the self-consistent DFT calculations. The rest of the calculation details are the same as described earlier in Section 2.3. Non-spin polarized *ab initio* band structure and its Wannier interpolation are shown in Fig. 3(b). One can see that the H_{TB} in this case also reproduces well the *ab initio* band structure.

After adding H_{soc} with parameters λ_p (for As-*p*) and λ_d (for Ta-*d*) to the H_{TB} forming $\mathcal{H}$, we fit the SOC included *ab initio* band structure with $\mathcal{H}$ in the next step. The fit is shown in Fig. 3(d). One can see that the fitting is quite good. This brings λ_p = 0.18 eV for and λ_d = 0.21 eV, which is in close agreement with the values for Ta atoms as reported in Ref. [65]. For lending support to the reliability of our estimated values of λ's and thusly obtained full Hamiltonian $\mathcal{H}$, the (001) terminated surface states of TaAs is calculated with this Hamiltonian using the iterative Green's function [66]. As shown in

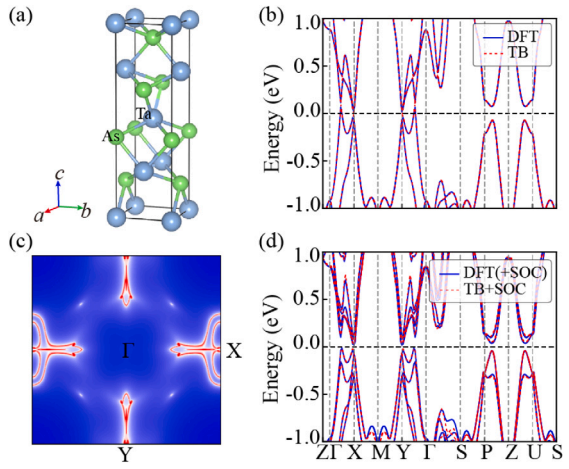


Fig. 3. (a) The body-centered-tetragonal crystals structure of TaAs. Light blue and green balls represent Ta and As atoms respectively. a, b and c are the crystallographic axes. (b) Wannier interpolation of the non-spin polarized *ab initio* band structure of TaAs to obtain H_{TB}. All the five Ta-d and three As-p orbitals are considered in the basis. (c) The (001) surface states are calculated using the $\mathcal{H}$ Hamiltonian. (d) Fitting of the SOC included *ab initio* band structure with $\mathcal{H}$. Fermi energy is set to zero.

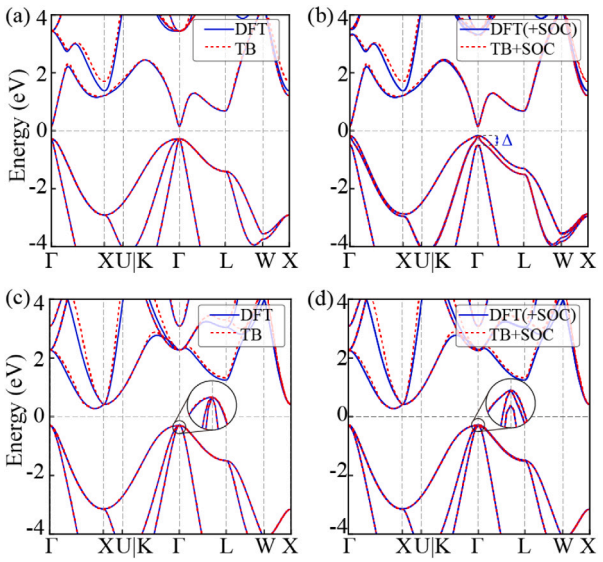


Fig. 4. Band structures from non-spin polarized DFT calculations and the Wannier tight-binding model H_{TB} for GaAs (a) and Si (c) cases. (b) Band structures from SOC included DFT band structure and the spin full tight-binding model $H_{\mathrm{TB}} + H_{\mathrm{soc}}$ for GaAs (b) and Si (d) cases. The Δ in (b) marks the spin–orbit splitting at Γ point. The inserts in (c) and (d) are to show the zoom-in of spin–orbit splitting at Γ point of the Si case. Fermi energy is set to zero.

Fig. 3(c), a spoon-shaped surface states around the X, and Y points appear on the surface Brillouin zone. Along Γ-X and Γ-Y directions, the Fermi-arc states connect and terminate at the Weyl points, which agrees well with the reported results from literature [15].

3.3. The case of semiconductors

For the sake of completeness and to further demonstrate the sensitivity of our method, in this section, we consider two examples of semiconductors GaAs and Si in which SOC strength supposedly varies significantly. Following the same procedure mentioned in Section 2, the SOC strength is estimated for these semiconductors.

Both the GaAs and Si crystallize in the diamond-type structure with the space group $F-43m$. The non-spin polarized *ab initio* calculations were performed within VASP package and Wannier90 interface to get the H_{TB} model. The plane-wave energy cutoff is 500 eV and k-grid is $8 \times 8 \times 8$ in the DFT calculation for both two cases. The rest of the calculation details are the same as described earlier in Section 2.3. Ga and As p orbitals in GaAs and p orbitals in Si are considered to be the SOC active orbital in the two cases and hence are considered in our TB basis.

The non-spin polarized *ab initio* band structure and its Wannier interpolation are shown in Fig. 4(a) and (c) for GaAs and Si respectively, where the H_{TB} reproduces the band structures very well in both the cases. The blue solid lines in Fig. 4(b) are the *ab initio* band structure of GaAs system with SOC effects considered self-consistently. The spin–orbit split band structure can be clearly observed especially at the Γ point for GaAs in Fig. 4(b), where the splitting at the top of the valence band is $\Delta \sim 0.328$ eV. By adding the onsite SOC Hamiltonian H_{soc} with the fitting parameters λ_p^{Ga} (for Ga) and λ_p^{As} (for As) to the non-spin polarized Hamiltonian H_{TB}, we obtain the spin-full Hamiltonian $\mathcal{H}$ that reproduce the SOC band structure quite well with $\lambda_p^{\mathrm{Ga}} = 0.157$ eV and $\lambda_p^{\mathrm{As}} = 0.209$ eV. The corresponding splitting energy at the top of the valence band from Hamiltonian $\mathcal{H}$ is $\Delta = 0.304$ eV, which matches pretty well with the DFT results.

As for the Si case, the negligibly small SOC effects are usually ignored when examining its properties. Fig. 4(d) shows the SOC *ab initio* band structure where the spin–orbit splitting can be barely seen. Therefore, we zoom it in the inset Fig. 4(d) to show the splitting energy $\Delta \sim 0.047$ eV at the top of the valence band. The SOC strength obtained from the best fit is $\lambda = 0.03$ eV, which generates the splitting of $\Delta = 0.045$ eV and matches quite well with the DFT result. Thus, we find the SOC strength to be moderate in GaAs but negligibly small in Si. Application of our method to GaAs and Si cases, in which SOC strength values significantly differ, again demonstrates the success of our approach in accurately estimating the SOC interaction strength.

Table 2
Comparison of SOC strengths (unit eV) estimated for example materials considered in this work. Wherever possible, we provide three values of SOC strength, namely from TBSOC, experimental estimation (Expt.) and from a recent theoretical estimation (Calc.). One can observe from the table that our estimated values are quite close to previously estimated experimental and theoretical values.

Systems	Orb.	TBSOC	Expt.	Calc. [32]
α-$RuCl_3$	Ru^{+3}-$4d^5$	0.120	0.096 [49]	0.143 (Ru)
Na_2IrO_3	Ir^{+4}-$5d^5$	0.380	0.378 [59]	0.514 (Ir)
$Na_2TeCo_2O_6$	Co^{+2}-$3d^7$	0.065	0.015 [50]	0.088 (Co)
TaAs	Ta^{+3}-$5d^2$	0.210	–	0.248 (Ta)
	As^{-3}-$4p^6$	0.180	0.190 (As) [67]	0.251 (As)
GaAs	Ga^{+3}-p	0.157	0.110 (Ga^{+1}) [67]	0.107 (Ga)
	As^{-3}-p	0.209	0.200 (As^{+1}) [67]	0.251 (As)
Si	p	0.030	–	0.030 (Si)

4. Comparison with literature

For comparison purposes, we list the SOC strengths in Table 2 estimated from TBSOC along with experimental estimates and a recent theoretical estimation for the elements considered as examples in this work.

5. Conclusion

We have presented a computational framework named TBSOC [36] to estimate the strength of SOC in solid-state materials. Our methodology is based on the combination of *ab initio* and tight-binding methods. To show its wider applicability, as case studies, we have considered

Table A.1
List of all the symbols used in main-text.

$\mathcal{H}$	spin-full TB Hamiltonian
H_{TB}	non-spin polarized TB Hamiltonian
H_{soc}	onsite SOC interaction
i, j	atom/site indices
α, β	atomic orbitals
$T_{i\alpha,i\alpha}$	onsite elements in H_{TB}
$T_{i\alpha,j\beta}$	hopping elements in H_{TB}
ℓ	angular quantum number
m	magnetic quantum number
Y_{ℓ}^{m}	spherical harmonics
$X_{\ell m}$	cubic harmonics
$\boldsymbol{J}$	total angular momentum
$\boldsymbol{L}$	orbital momentum
L_z	z-component orbital operator
$L_{\pm}$	raising and lowering orbital operators
$\boldsymbol{S}$	spin momentum
S_z	z-component spin operator
$S_{\pm}$	raising and lowering spin operators
λ	spin–orbit coupling strength

transition metal compounds α-$RuCl_3$, $Na_2TeCo_2O_6$ and Na_2IrO_3, a topological weyl semi-metal TaAs system and example of two semiconductors Si and GaAs. We demonstrated the ability of our TBSOC in well reproducing the self-consistent SOC included *ab initio* band structures. This has been done employing a TB model H_{TB} with the addition of onsite SOC term H_{soc}. We show that it works well in both cases, materials with strong and weak SOC interactions, covering a broad range of materials. We also show that TBSOC works for both local and global coordinate systems, making its utility smoother for further analysis and employment in successive model calculations. This simplistic approach can readily be applied to a wide range of materials.

CRediT authorship contribution statement

Qiangqiang Gu: Conceptualization, Methodology, Software, Validation, Formal analysis, Visualization, Writing – original draft, Writing – review & editing. **Shishir Kumar Pandey:** Methodology, Validation, Formal analysis, Visualization, Writing – original draft, Writing – review & editing. **Rajarshi Tiwari:** Software, Writing – original draft.

Declaration of competing interest

The authors declare that they have no known competing financial interests or personal relationships that could have appeared to influence the work reported in this paper.

Data availability

Data will be made available on request.

Acknowledgments

This work is supported partially by the China Postdoctoral Science Foundation (No. 2022M710231) awarded to Q. Gu. We also acknowledge the support of computing resource provided by the Bohrium Cloud Platform (https://bohrium.dp.tech) from DP Technology.

Appendix. Table of symbols

Here we list all the important symbols and physical parameters used in the main text. (See Table A.1.)

References

[1] B.G. Park, J. Wunderlich, D.A. Williams, S.J. Joo, K.Y. Jung, K.H. Shin, K. Olejník, A.B. Shick, T. Jungwirth, Tunneling anisotropic magnetoresistance in multilayer-(Co/Pt)/AlO_x/Pt structures, Phys. Rev. Lett. 100 (2008) 087204.
[2] D.D. Scherer, B.M. Andersen, Spin–orbit coupling and magnetic anisotropy in iron-based superconductors, Phys. Rev. Lett. 121 (3) (2018) 037205.
[3] F. Waßer, A. Schneidewind, Y. Sidis, S. Wurmehl, S. Aswartham, B. Büchner, M. Braden, Spin reorientation in $Ba_{0.65}Na_{0.35}Fe_2As_2$ studied by single-crystal neutron diffraction, Phys. Rev. B 91 (2015) 060505.
[4] J. Sinova, S.O. Valenzuela, J. Wunderlich, C.H. Back, T. Jungwirth, Spin Hall effects, Rev. Modern Phys. 87 (2015) 1213–1260.
[5] A. Vedyayev, N. Ryzhanova, N. Strelkov, B. Dieny, Spontaneous anomalous and spin Hall effects due to spin–orbit scattering of evanescent wave functions in magnetic tunnel junctions, Phys. Rev. Lett. 110 (2013) 247204.
[6] M.Y. Zhuravlev, A. Alexandrov, L. Tao, E.Y. Tsymbal, Tunneling anomalous Hall effect in a ferroelectric tunnel junction, Appl. Phys. Lett. 113 (17) (2018) 172405.
[7] A. Matos-Abiague, J. Fabian, Tunneling anomalous and spin Hall effects, Phys. Rev. Lett. 115 (2015) 056602.
[8] A. Vedyayev, M. Titova, N. Ryzhanova, M.Y. Zhuravlev, E.Y. Tsymbal, Anomalous and spin Hall effects in a magnetic tunnel junction with Rashba spin–orbit coupling, Appl. Phys. Lett. 103 (3) (2013) 032406.
[9] M. König, S. Wiedmann, C. Brüne, A. Roth, H. Buhmann, L.W. Molenkamp, X.L. Qi, S.C. Zhang, Quantum spin Hall insulator state in HgTe quantum wells, Science 318 (5851) (2007) 766–770.
[10] D. Hsieh, D. Qian, L. Wray, Y. Xia, Y.S. Hor, R.J. Cava, M.Z. Hasan, A topological Dirac insulator in a quantum spin Hall phase, Nature 452 (7190) (2008) 970–974.
[11] D. Hsieh, Y. Xia, D. Qian, L. Wray, F. Meier, J. Osterwalder, L. Patthey, J.G. Checkelsky, N. Ong, A.V. Fedorov, et al., A tunable topological insulator in the spin helical Dirac transport regime, Nature 460 (7259) (2009) 1101–1105.
[12] D. Hsieh, Y. Xia, D. Qian, L. Wray, F. Meier, J.H. Dil, J. Osterwalder, L. Patthey, A.V. Fedorov, H. Lin, A. Bansil, D. Grauer, Y.S. Hor, R.J. Cava, M.Z. Hasan, Observation of time-reversal-protected single-Dirac-Cone topological-insulator states in Bi_2Te_3 and Sb_2Te_3, Phys. Rev. Lett. 103 (2009) 146401.
[13] Y.L. Chen, J.G. Analytis, J.-H. Chu, Z.K. Liu, S.-K. Mo, X.L. Qi, H.J. Zhang, D.H. Lu, X. Dai, Z. Fang, S.C. Zhang, I.R. Fisher, Z. Hussain, Z.-X. Shen, Experimental realization of a three-dimensional topological insulator Bi_2Te_3, Science 325 (5937) (2009) 178–181.
[14] X. Wan, A.M. Turner, A. Vishwanath, S.Y. Savrasov, Topological semimetal and Fermi-arc surface states in the electronic structure of pyrochlore iridates, Phys. Rev. B 83 (2011) 205101.
[15] H. Weng, C. Fang, Z. Fang, B.A. Bernevig, X. Dai, Weyl semimetal phase in noncentrosymmetric transition-metal monophosphides, Phys. Rev. X 5 (1) (2015).
[16] A.A. Soluyanov, D. Gresch, Z. Wang, Q. Wu, M. Troyer, X. Dai, B.A. Bernevig, Type-II.Weyl semimetals, Nature 527 (7579) (2015) 495–498.
[17] B. Kim, H. Ohsumi, T. Komesu, S. Sakai, T. Morita, H. Takagi, T.-h. Arima, Phase-sensitive observation of a spin–orbital mott state in Sr_2IrO_4, Science 323 (5919) (2009) 1329–1332.
[18] Y. Maeno, H. Hashimoto, K. Yoshida, S. Nishizaki, T. Fujita, J. Bednorz, F. Lichtenberg, Superconductivity in a layered perovskite without copper, Nature 372 (6506) (1994) 532–534.
[19] G. Khaliullin, W. Koshibae, S. Maekawa, Low energy electronic states and triplet pairing in layered cobaltate, Phys. Rev. Lett. 93 (2004) 176401.
[20] B.J. Kim, H. Jin, S.J. Moon, J.-Y. Kim, B.-G. Park, C.S. Leem, J. Yu, T.W. Noh, C. Kim, S.J. Oh, J.-H. Park, V. Durairaj, G. Cao, E. Rotenberg, Novel J_{eff} =1/2 mott state induced by relativistic spin-orbit coupling in Sr_2IrO_4, Phys. Rev. Lett. 101 (2008) 076402.
[21] G. Khaliullin, Orbital order and fluctuations in Mott insulators, Progr. Theoret. Phys. Suppl. 160 (2005) 155–202.
[22] G. Jackeli, G. Khaliullin, Mott insulators in the strong spin–orbit coupling limit: From Heisenberg to a quantum compass and Kitaev models, Phys. Rev. Lett. 102 (1) (2009) 017205.
[23] N. Zibouche, A. Kuc, J. Musfeldt, T. Heine, Transition-metal dichalcogenides for spintronic applications, Ann. Phys. 526 (9-10) (2014) 395–401.
[24] A. Georges, L. d. Medici, J. Mravlje, Strong correlations from Hund's coupling, Annu. Rev. Condens. Matter Phys. 4 (1) (2013) 137–178.
[25] C.L. Kane, E.J. Mele, Quantum spin Hall effect in graphene, Phys. Rev. Lett. 95 (2005) 226801.
[26] S.K. Pandey, Q. Gu, R. Tiwari, Emergence of bond-dependent highly anisotropic magnetic interactions in Sr_4RhO_6: A theoretical study, 2022, arXiv preprint arXiv:2207.05045.

[27] S.K. Pandey, J. Feng, Spin interaction and magnetism in cobaltate kitaev candidate materials: An *ab initio* and model hamiltonian approach, Phys. Rev. B 106 (2022) 174411.

[28] S.L. Adler, Quantum theory of the dielectric constant in real solids, Phys. Rev. 126 (1962) 413–420.

[29] N. Wiser, Dielectric constant with local field effects included, Phys. Rev. 129 (1963) 62–69.

[30] F. Aryasetiawan, M. Imada, A. Georges, G. Kotliar, S. Biermann, A.I. Lichtenstein, Frequency-dependent local interactions and low-energy effective models from electronic structure calculations, Phys. Rev. B 70 (2004) 195104.

[31] N. Marzari, A.A. Mostofi, J.R. Yates, I. Souza, D. Vanderbilt, Maximally localized Wannier functions: Theory and applications, Rev. Modern Phys. 84 (4) (2012) 1419–1475.

[32] G. Jha, T. Heine, DFTB parameters for the periodic table: Part III spin-orbit coupling, J. Chem. Theory Comput. 18 (7) (2022) 4472–4481.

[33] R. Cuadrado, R. Robles, A. García, M. Pruneda, P. Ordejón, J. Ferrer, J.I. Cerdá, Validity of the on-site spin–orbit coupling approximation, Phys. Rev. B 104 (2021) 195104.

[34] K. Kurita, T. Koretsune, Systematic first-principles study of the on-site spin–orbit coupling in crystals, Phys. Rev. B 102 (2020) 045109.

[35] M. Vijayakumar, M. Gopinathan, Spin–orbit coupling constants of transition metal atoms and ions in density functional theory, THEOCHEM 361 (1) (1996) 15–19.

[36] Q. Gu, TBSOC, 2020, https://github.com/qqgu/TBSOC.

[37] J.A. Nelder, R. Mead, A simplex method for function minimization, Comput. J. 7 (4) (1965) 308–313.

[38] F. Gao, L. Han, Implementing the Nelder–Mead simplex algorithm with adaptive parameters, Comput. Optim. Appl. 51 (1) (2012) 259–277.

[39] A.A. Mostofi, J.R. Yates, Y.S. Lee, I. Souza, D. Vanderbilt, N. Marzari, Wannier90: A tool for obtaining maximally-localised Wannier functions, Comput. Phys. Comm. 178 (9) (2008) 685–699.

[40] G. Kresse, J. Furthmüller, Efficient iterative schemes for *ab initio* total-energy calculations using a plane-wave basis set, Phys. Rev. B 54 (1996) 11169–11186.

[41] G. Kresse, D. Joubert, From ultrasoft pseudopotentials to the projector augmented-wave method, Phys. Rev. B 59 (1999) 1758–1775.

[42] P.E. Blöchl, Projector augmented-wave method, Phys. Rev. B 50 (1994) 17953–17979.

[43] J.P. Perdew, K. Burke, M. Ernzerhof, Generalized gradient approximation made simple, Phys. Rev. Lett. 77 (1996) 3865–3868.

[44] S.M. Winter, Y. Li, H.O. Jeschke, R. Valentí, Challenges in design of Kitaev materials: Magnetic interactions from competing energy scales, Phys. Rev. B 93 (2016) 214431.

[45] R.D. Johnson, S.C. Williams, A.A. Haghighirad, J. Singleton, V. Zapf, P. Manuel, I.I. Mazin, Y. Li, H.O. Jeschke, R. Valentí, R. Coldea, Monoclinic crystal structure of α-$RuCl_3$ and the zigzag antiferromagnetic ground state, Phys. Rev. B 92 (2015) 235119.

[46] H.B. Cao, A. Banerjee, J.-Q. Yan, C.A. Bridges, M.D. Lumsden, D.G. Mandrus, D.A. Tennant, B.C. Chakoumakos, S.E. Nagler, Low-temperature crystal and magnetic structure ofα-$RuCl_3$, Phys. Rev. B 93 (2016) 134423.

[47] K. Brodersen, G. Thiele, H. Ohnsorge, I. Recke, F. Moers, Die struktur des IrBr3 und über die ursachen der fehlordnungserscheinungen bei den in schichtenstrukturen kristallisierenden edelmetalltrihalogeniden, J. Less Common Metals 15 (3) (1968) 347–354.

[48] K.W. Plumb, J.P. Clancy, L.J. Sandilands, V.V. Shankar, Y.F. Hu, K.S. Burch, H.-Y. Kee, Y.-J. Kim, α-$RuCl_3$: A spin–orbit assisted mott insulator on a honeycomb lattice, Phys. Rev. B 90 (2014) 041112.

[49] L.J. Sandilands, Y. Tian, A.A. Reijnders, H.-S. Kim, K.W. Plumb, Y.-J. Kim, H.-Y. Kee, K.S. Burch, Spin–orbit excitations and electronic structure of the putative Kitaev magnet α-$RuCl_3$, Phys. Rev. B 93 (2016) 075144.

[50] M. Songvilay, J. Robert, S. Petit, J.A. Rodriguez-Rivera, W.D. Ratcliff, F. Damay, V. Balédent, M. Jiménez-Ruiz, P. Lejay, E. Pachoud, A. Hadj-Azzem, V. Simonet, C. Stock, Kitaev interactions in the Co honeycomb antiferromagnets $Na_3Co_2SbO_6$ and $Na_2Co_2TeO_6$, Phys. Rev. B 102 (2020) 224429.

[51] L. Viciu, Q. Huang, E. Morosan, H. Zandbergen, N. Greenbaum, T. McQueen, R. Cava, Structure and basic magnetic properties of the honeycomb lattice compounds $Na_2Co_2TeO_6$ and $Na_3Co_2SbO_6$, J. Solid State Chem. 180 (3) (2007) 1060–1067.

[52] W. Chen, X. Li, Z. Hu, Z. Hu, L. Yue, R. Sutarto, F. He, K. Iida, K. Kamazawa, W. Yu, X. Lin, Y. Li, Spin–orbit phase behavior of $Na_2Co_2TeO_6$ at low temperatures, Phys. Rev. B 103 (2021) L180404.

[53] G. Xiao, Z. Xia, W. Zhang, X. Yue, S. Huang, X. Zhang, F. Yang, Y. Song, M. Wei, H. Deng, et al., Crystal growth and the magnetic properties of $Na_2Co_2TeO_6$ with quasi-two-dimensional honeycomb lattice, Cryst. Growth Des. 19 (5) (2019) 2658–2662.

[54] E. Lefrançois, M. Songvilay, J. Robert, G. Nataf, E. Jordan, L. Chaix, C.V. Colin, P. Lejay, A. Hadj-Azzem, R. Ballou, V. Simonet, Magnetic properties of the honeycomb oxide $Na_2Co_2TeO_6$, Phys. Rev. B 94 (2016) 214416.

[55] A.K. Bera, S.M. Yusuf, A. Kumar, C. Ritter, Zigzag antiferromagnetic ground state with anisotropic correlation lengths in the quasi-two-dimensional honeycomb lattice compound $Na_2Co_2TeO_6$, Phys. Rev. B 95 (2017) 094424.

[56] Y. Singh, S. Manni, J. Reuther, T. Berlijn, R. Thomale, W. Ku, S. Trebst, P. Gegenwart, Relevance of the Heisenberg-Kitaev model for the honeycomb lattice iridates A_2IrO_3, Phys. Rev. Lett. 108 (2012) 127203.

[57] Y. Singh, P. Gegenwart, Antiferromagnetic mott insulating state in single crystals of the honeycomb lattice material Na_2IrO_3, Phys. Rev. B 82 (2010) 064412.

[58] S.K. Choi, R. Coldea, A.N. Kolmogorov, T. Lancaster, I.I. Mazin, S.J. Blundell, P.G. Radaelli, Y. Singh, P. Gegenwart, K.R. Choi, S.-W. Cheong, P.J. Baker, C. Stock, J. Taylor, Spin waves and revised crystal structure of honeycomb iridate Na_2IrO_3, Phys. Rev. Lett. 108 (2012) 127204.

[59] O.F. Schirmer, A. Forster, H. Hesse, M. Wohlecke, S. Kapphan, Paramagnetic resonance and near-infrared optical absorption of $SrTiO_3$:Ir^{4+}, J. Phys. C: Solid State Phys. 17 (7) (1984) 1321.

[60] B.Q. Lv, H.M. Weng, B.B. Fu, X.P. Wang, H. Miao, J. Ma, P. Richard, X.C. Huang, L.X. Zhao, G.F. Chen, Z. Fang, X. Dai, T. Qian, H. Ding, Experimental discovery of Weyl Semimetal TaAs, Phys. Rev. X 5 (3) (2015).

[61] X. Zheng, Q. Gu, Y. Liu, B. Tong, J.-F. Zhang, C. Zhang, S. Jia, J. Feng, R.R. Du, Observation of 1D Fermi arc states in Weyl semimetal TaAs, Natl. Sci. Rev. 9 (8) (2022) nwab191.

[62] H. Inoue, A. Gyenis, Z. Wang, J. Li, S.W. Oh, S. Jiang, N. Ni, B.A. Bernevig, A. Yazdani, Quasiparticle interference of the Fermi arcs and surface-bulk connectivity of a Weyl semimetal, Science 351 (6278) (2016) 1184–1187.

[63] X. Huang, L. Zhao, Y. Long, P. Wang, D. Chen, Z. Yang, H. Liang, M. Xue, H. Weng, Z. Fang, X. Dai, G. Chen, Observation of the Chiral-Anomaly-Induced negative magnetoresistance in 3D Weyl semimetal TaAs, Phys. Rev. X 5 (2015) 031023.

[64] G.B. Osterhoudt, L.K. Diebel, M.J. Gray, X. Yang, J. Stanco, X. Huang, B. Shen, N. Ni, P.J.W. Moll, Y. Ran, K.S. Burch, Colossal mid-infrared bulk photovoltaic effect in a type-I Weyl semimetal, Nature Mater. 18 (5) (2019) 471–475.

[65] K.V. Shanavas, S. Popović, S. Satpathy, Theoretical model for Rashba spin–orbit interaction in *d* electrons, Phys. Rev. B 90 (2014) 165108.

[66] M.P.L. Sancho, J.M.L. Sancho, J.M.L. Sancho, J. Rubio, Highly convergent schemes for the calculation of bulk and surface Green functions, J. Phys. F: Met. Phys. 15 (4) (1985) 851–858.

[67] K. Wittel, R. Manne, Atomic spin–orbit interaction parameters from spectral data for 19 elements, Theor. Chim. Acta 33 (4) (1974) 347–349.